4 SEPTEMBER 2024

Science Translational Medicine

AAAS

DEVICES

A skin-interfaced microfluidic platform supports dynamic sweat biochemical analysis during human exercise

Soongwon Cho[1,2]†, Samy M. Shaban[3,4,5]†, Ruihao Song[1,6]†, Haohui Zhang[7]†, Dasom Yang[1,8]†, Min-Jae Kim[3,4], Yirui Xiong[1,9], Xiuyuan Li[7], Kenneth Madsen[2,10], Sarena Wapnick[11], Shifan Zhang[12], Ziyu Chen[9], Jiwon Kim[1,2,3], Gianna Guinto[13], Michelle Li[11], Minkyu Lee[1,14,15], Ravi F. Nuxoll[1,9,16], Shaghayegh Shajari[1,2], Jin Wang[1,2,9,17], Seongeun Son[18], Jihoon Shin[3,4], Alexander J. Aranyosi[1,2,19], Donald E. Wright[19], Tae-il Kim[3,4], Roozbeh Ghaffari[1,2,11,19], Yonggang Huang[1,7,9,20]*, Dong-Hwan Kim[3,4]*, John A. Rogers[1,2,9,11,21]*

Blood lactate concentration is an established circulating biomarker for measuring muscle acidity and can be evaluated for monitoring endurance, training routines, or athletic performance. Sweat is an alternative biofluid that may serve similar purposes and offers the advantage of noninvasive collection and continuous monitoring. The relationship between blood lactate and dynamic sweat biochemistry for wearable engineering applications in physiological fitness remains poorly defined. Here, we developed a microfluidic wearable band with an integrated colorimetric timer and biochemical assays that temporally captures sweat and measures pH and lactate concentration. A colorimetric silver nanoplasmonic assay was used to measure the concentration of lactate, and dye-conjugated SiO_2 nanoparticle–agarose composite materials supported dynamic pH analysis. We evaluated these sweat biomarkers in relation to blood lactate in human participant studies during cycling exercise of varying intensity. Iontophoresis-generated sweat pH from regions of actively working muscles decreased with increasing heart rate during exercise and was negatively correlated with blood lactate concentration. In contrast, sweat pH from nonworking muscles did not correlate with blood lactate concentration. Changes in sweat pH and blood lactate were observed in participants who did not regularly exercise but not in individuals who regularly exercised, suggesting a relationship to physical fitness and supporting further development for noninvasive, biochemical fitness evaluations.

INTRODUCTION

Skin-interfaced wearable biochemical sensors are of interest for their ability to provide information on physiological status for a range of health-related applications including the monitoring of exercise and endurance. These sensors typically require access to a biofluid such as sweat, tears, or interstitial fluid to provide biochemical measurements. Muscle pH is a metric of muscle fatigue for sports physiology because the dominant anaerobic respiration pathway results in progressive acidosis during intense exercise (*1*–*3*); however, monitoring muscle pH requires invasive needle biopsies, limiting its practical usefulness. Blood lactate is strongly correlated with muscle metabolic acidosis and offers a less invasive approach for investigating muscle fatigue. Blood analysis, however, requires discrete sampling events and skin penetration with the associated risks of pain and infection (*4*–*6*). Interstitial fluid analysis not only has the potential to continuously evaluate lactate concentration similar to existing blood glucose technology (*7*–*9*) but also requires skin puncture by microneedles. Sweat can serve as an alternative to blood for certain diagnostic assessments, with the benefits of noninvasive and continuous collection during physical activity. Sweat pH and lactate concentrations have been examined for evaluation of sports physiology (*4*–*6*, *10*–*12*); however, there is a need to establish quantitative comparisons of sweat analytes with corresponding gold-standard parameters in peripheral blood and muscle tissue.

Sweat analysis by skin-interfaced wireless devices has incorporated electrochemical (*10*, *13*–*15*), colorimetric (*16*–*18*), or hybrid sensors (*19*), some with capabilities to capture and handle sweat for real-time in situ quantitative analysis. Microfluidic designs with colorimetric sensors are attractive because of their simplicity in design and versatility in function (*20*, *21*), but they lack a convenient

[1]Querrey Simpson Institute for Bioelectronics, Northwestern University, Evanston, IL 60208, USA. [2]Center for Bio-Integrated Electronics, Northwestern University, Evanston, IL 60208, USA. [3]School of Chemical Engineering, Sungkyunkwan University, Suwon, 16419, Republic of Korea. [4]Biomedical Institute for Convergence at SKKU (BICS), Sungkyunkwan University, Suwon, 16419, Republic of Korea. [5]Petrochemical Department, Egyptian Petroleum Research Institute, Cairo, 11727, Egypt. [6]Department of Chemical and Biological Engineering, Northwestern University, Evanston, IL 60208, USA. [7]Departments of Civil and Environmental Engineering, Northwestern University, Evanston, IL 60208, USA. [8]Precision Biology Research Center (PBRC), Sungkyunkwan University, Suwon, 16419, Republic of Korea. [9]Departments of Material Science and Engineering, Northwestern University, Evanston, IL 60208, USA. [10]Department of Chemistry, University of Illinois at Urbana-Champaign, Urbana, IL 61801, USA. [11]Department of Biomedical Engineering, Northwestern University, Evanston, IL 60208, USA. [12]Department of Statistics, School of Computer, Data and Information Sciences, University of Wisconsin-Madison, Madison, WI 53706, USA. [13]College of Science and Health, DePaul University, Chicago, IL 60614, USA. [14]Shirley Ryan AbilityLab, Chicago, IL 60611, USA. [15]Department of Physical Medicine and Rehabilitation, Northwestern University, Chicago, IL 60611, USA. [16]Department of Physics and Astronomy, Northwestern University, Evanston, IL 60208, USA. [17]Pritzker School of Molecular Engineering, University of Chicago, Chicago, IL 60637, USA. [18]Department of Bionano Engineering, Center for Bionano Intelligence Education and Research, Hanyang University, Ansan, 15588, Republic of Korea. [19]Epicore Biosystems, Cambridge, MA 02139, USA. [20]Department of Mechanical Engineering, Northwestern University, Evanston, IL 60208, USA. [21]Department of Neurological Surgery, Northwestern University, Evanston, IL 60208, USA.
*Corresponding author. Email: y-huang@northwestern.edu (Y.H.); dhkim1@skku.edu (D.-H.K.); jrogers@northwestern.edu (J.A.R.)
†These authors contributed equally to this work.

means to track time-dynamic characteristics or to accurately monitor key biochemical metabolic species, such as pH and lactate. The technology platforms introduced here support timed measurements of sweat chemistry through an elastic microfluidic band that integrates a suite of colorimetric sensors and timers for studies of sweat pH and lactate in human exercise. The system was designed to allow continuous sweat collection from the surface of the skin and time-dependent chemical analysis. Advanced functional components include a sweat-activated colorimetric timer based on the reactive diffusion of a maltodextrin-iodine complex, an interference-free nanoplasmonic lactate enzymatic sensor that produces multicolor changes through silver nanoplate (AgNPL) etching, a nonbleeding SiO_2 pH sensor based on bromothymol blue (BTB)–conjugated mesoporous nanoparticles, and a conventional thermochromic liquid crystal sensor. By digital image acquisition and analysis, each assay allows colorimetric quantification and temporal tracking of biomarker concentrations in a wireless fashion without any supporting electronics or power supplies. The band supports a reusable, adhesive-free, water-tight interface to the skin, with the ability to collect sweat from the wrist, forearm, ankle, or other body parts.

The skin-interfaced microfluidic band developed here was tested in a series of human participants during rest or physical activity and in parallel with blood metabolite analysis. The results support a technologically minimalist, cost-effective means for tracking time-dynamic changes in sweat composition with body location, exercise type, duration, and intensity. Because of the wearable nature of the device, we were able to measure sweat pH in both working and nonworking muscles, which showed different responses to exercise, providing insights into local muscle activity. Our findings suggest that sweat pH may offer a noninvasive alternative for assessing changes in muscle acidity, given that sweat pH correlates with blood lactate. Human participant studies indicate a potential for differentiation of personal fitness status, whereby participants who regularly exercise maintain sweat pH homeostasis better than participants who do not regularly exercise. Our data suggest possibilities for routine use of sweat monitoring in personal fitness and create opportunities for similar studies of other important chemical species in sweat.

RESULTS

A skin-interfaced microfluidic elastic band captures sweat for biochemical analyses

Here, we designed a microfluidic band and colorimetric sensor suite for adhesive-free monitoring of sweat biochemical analytes (Fig. 1A). The elastomer poly(dimethylsiloxane) (PDMS) constituted the body of the device covered by a film of PDMS and polyethylene terephthalate (PET). An elastic rubber strap secured with a "snap and loop" fastener secured the device to the body with options to integrate with smartwatches (fig. S1A). The PDMS band has a skin-interfacing inlet, formed by lightly cross-linked PDMS (30:1 ratio), connected to molded sweat collection chambers (Fig. 1B and fig. S1B). This inlet routed sweat through to an enclosed linear series of microfluidic channels, valves, and reservoirs with colorimetric chemical reagents (Fig. 1, B and C). To evaluate the interaction of this inlet with human skin, the soft PDMS sweat collection well was gently pressed against the forearm of a human participant (fig. S1C). The well remained attached under gentle pulling of the device away from the skin, indicating a tacky interface (fig. S1D). To test whether the interface was water tight, the band was worn on the wrist with a food dye–loaded cellulose paper placed at the inlet (fig. S1E). The device left a localized dye mark on the skin inside the inlet area indicating a water-tight interface (fig. S1, F and G), whereas when leakage was artificially induced, the dye mark was visible outside of the inlet area (fig. S1, H and I). The band can be worn on the wrist, forearm, or ankle by stretching the band around the targeted body part (Fig. 1, D and E). The ability of the band to adhere to the skin without leakage suggested that there is no need for an additional adhesive component, which has an associated risk of skin irritation (*22*).

To evaluate strain in the band under stretching, bending, or twisting, we conducted finite element analysis (FEA) of the distribution of the maximum principal strain on the external surface of the PDMS microfluidics (Fig. 1, F to H). The PDMS body of the device has an approximate elastic modulus of 0.8 MPa (*23*) and fracture strain of about 80% (*23*), whereas the PET film cover has an approximate modulus of 2 GPa and fracture strain of 1.5% (*24*). An elastic rubber strap with an approximate modulus of 2 MPa was used to fasten the device to the body (fig. S1J). Under 10% stretch, FEA demonstrated that the rubber strap experienced a maximum principal strain of 54.3% (fig. S1J), whereas PDMS and PET reached only 4 and 1.3%, respectively (Fig. 1F and fig. S1, K and L). These findings indicated that the rubber strap absorbed most of the deformations in the device, thus mechanically isolating the PDMS and PET (fig. S1, J to L). With 120° bending, PDMS and PET exhibited 2.9 and 0.06% maximum principal strain, respectively (Fig. 1G). Under 120° twisting, PDMS and PET demonstrated 3.7 and 0.7% strain, respectively (Fig. 1H). Bending of 120° had negligible influence on the geometrical integrity of each of the microfluidic chambers (fig. S2A), changing their length and height by less than 1% (fig. S2, B and C). These microfluidic geometrical deformations under bending, twisting, and stretching had negligible influence on the timer sensor performance in the FEA model (fig. S2D).

Maltodextrin-iodine can be used as a colorimetric timer

To achieve a temporal characterization of sweat biomarker concentration, we designed a colorimetric readout assay for elapsed time using the controlled chemical dissociation of the colored maltodextrin-iodine and the diffusion of the dissociated iodine/iodide species. A cellulose fiber paper was loaded with the maltodextrin-iodine complex and phosphate buffer (pH 5.5) and then coated with a perfluorinated resin (Nafion) to form a core-shell fiber structure (fig. S3, A and B). Successful loading of maltodextrin-iodine and coating with Nafion, which acts as a glue for maltodextrin-iodine particles on the cellulose fiber, was confirmed by scanning electron microscopy with energy-dispersive x-ray spectroscopy (SEM-EDS) labeling iodine and fluorine (fig. S3, C and D). This paper-based assay was placed in a reservoir within the PDMS band and covered with the PDMS and PET film (Fig. 2A). The assay was designed such that sweat entering the reservoir from the skin should solubilize the purple maltodextrin-iodine complex, leading to complex dissociation, free iodine diffusion, and a loss of color in a time-dependent fashion (*25*). FEA simulations were constructed on the basis of the mass conservation of iodide, iodine, and maltodextrin to model the dissociation of maltodextrin-iodine and the diffusion of iodine/iodide through the device over a 60-min simulation (Fig. 2A and fig. S4, A to C). The model was designed to incorporate all relevant processes of chemical dissociation of the maltodextrin-iodine complex and diffusion of iodine/iodide through various materials and parameters of the system (Fig. 2, B to E, and table S1). The

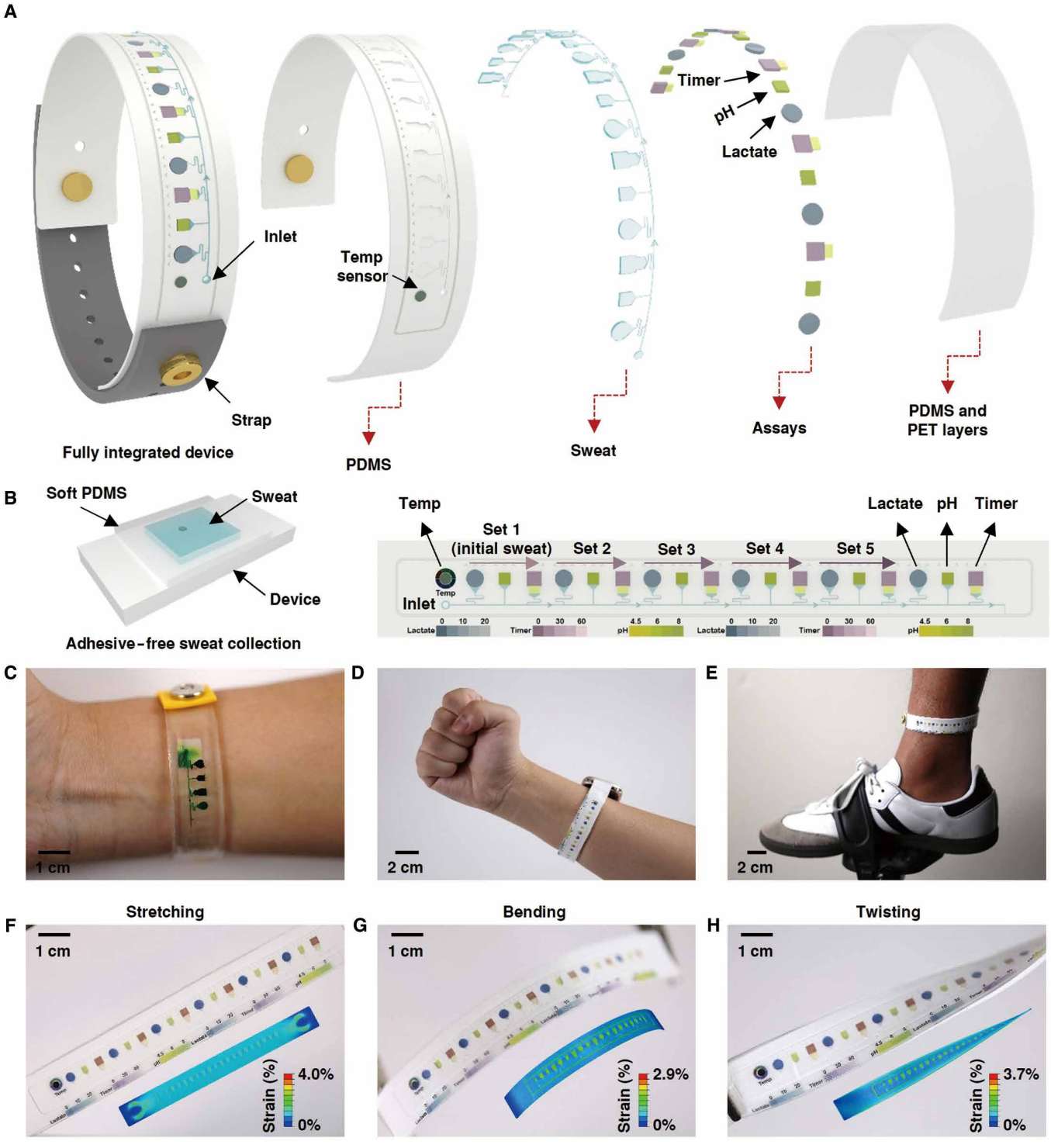

Fig. 1. Microfluidic skin-interfaced elastic band for sweat capture. (**A**) Schematic of the complete device and exploded view showing PDMS layer with temperature sensor, sweat collecting reservoirs, valves, and microfluidic channels; the array of colorimetric assays; and the PDMS and PET top layer. (**B**) Rendering of the sweat collection inlet region (left) and layout of the colorimetric assays, including temperature sensor (black circle), six sets of lactate sensor (blue circle), pH sensor (yellow square), and colorimetric timer (purple square) in series. Color scales, lactate (millimolar), timer (minutes), and pH. (**C**) Photograph of the microfluidic band on the skin with food dye visualization. Scale bar, 1 cm. (**D**) Representative image of the device worn on the wrist with a smartwatch interface and (**E**) the device worn on the ankle. Scale bar, 2 cm. (**F** to **H**) Representative simulations of FEA showing the distribution of the principal strain on the external surface of the PDMS microfluidic structure and the respective images during 10% stretching (F), 120° bending (G), and 120° twisting (H). Scale bars, 1 cm. Color scales, % strain. Renderings and illustrations created with Autodesk 3ds Max.

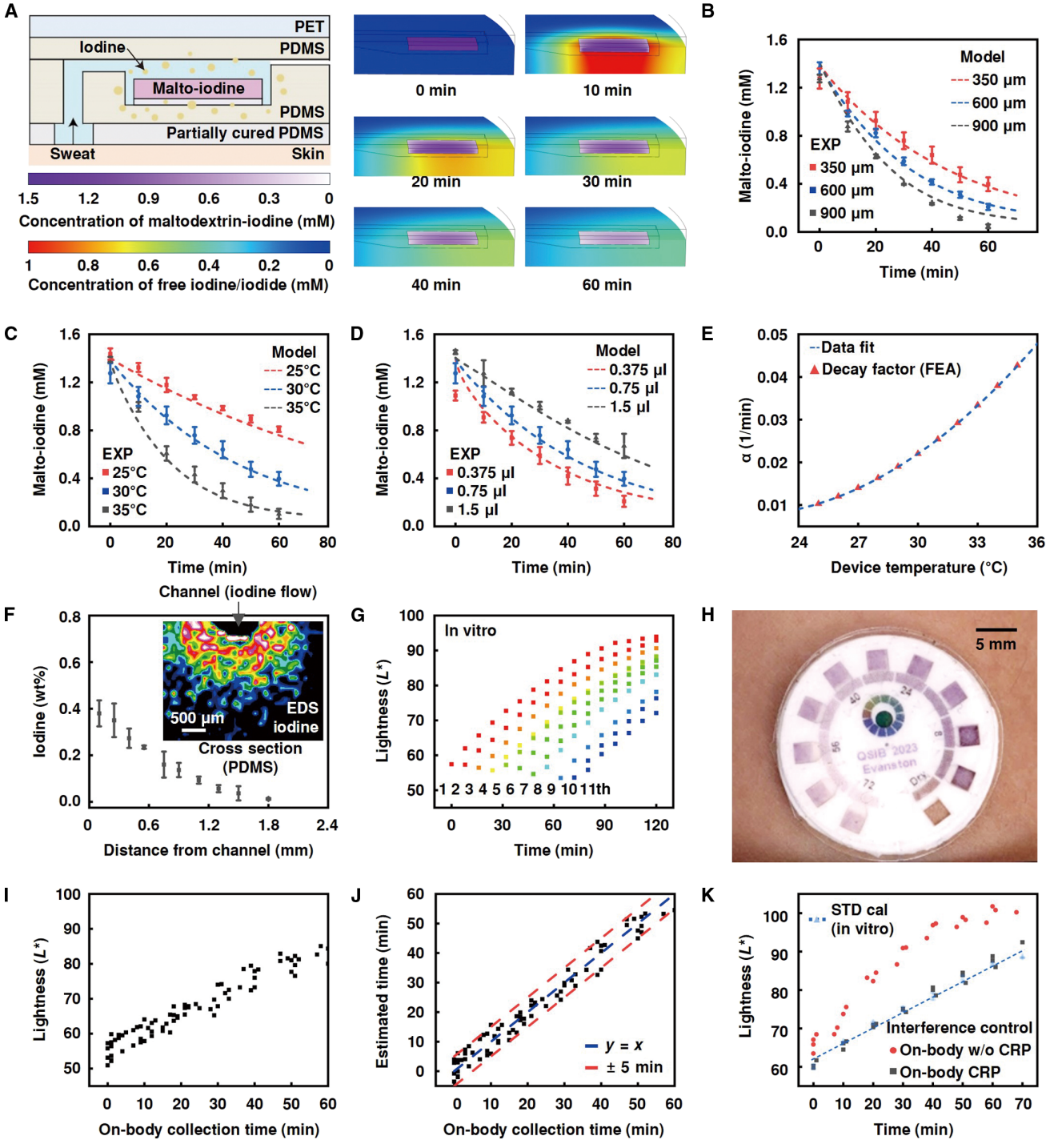

Fig. 2. Maltodextrin-iodine as a colorimetric timer. (**A**) Schematic illustration of the timer module inside a microfluidic reservoir (left) and FEA of the reactive diffusion processes from the cellulose to surrounding sweat and PDMS over 60 min (right). Color scale (top), maltodextrin-iodine concentration. Color scale (bottom), free iodine/iodide concentration. (**B** to **D**) Time dependence of the maltodextrin-iodine concentration for experimental (EXP) (squares) and simulation (dashed lines) data in different PDMS microfluidic chamber depths (B), temperatures (C), and Nafion amount (D). $n = 3$. (**E**) Temperature dependence of the decay factor (α) for maltodextrin-iodine. Data were fit to a parabolic curve. (**F**) Measure of iodine % weight within a cross section of a PDMS channel after flowing iodine solution for 16 hours. $n = 3$. Inset shows a visualization of iodine diffusion by energy dispersive spectroscopy (EDS). Scale bar, 500 µm. (**G**) Change in L^* over time for 11 colorimetric timers after sequential filling. $n = 11$. (**H**) Representative photograph of a colorimetric timer device during on-body use. Scale bar, 5 mm. (**I**) On-body measurements of the lightness of the timer as a function of time. $n = 10$ chambers. (**J**) Pearson correlation of estimated and actual sweat collection time over 10 chambers during on-body evaluations. Blue dotted line, target line. Red dotted line, ±5 min. $n = 109$ chambers. (**K**) Measurement of L^* response over time from on-body tests with (gray square) or without (red circle) CRPs or benchtop calibration data (blue dotted line). One-way ANOVA with Tukey's post hoc test. 40 min, $P = 0.0036$. $n = 3$. Illustrations created with Adobe Illustrator.

modeled dissociation rate increased with larger PDMS reservoir depths allowing more iodine to diffuse (Fig. 2B), increased temperature led to higher diffusivity and dissociation (Fig. 2C), and increasing thicknesses of the Nafion coatings led to less diffusivity (Fig. 2D). The time (t) dependence of the maltodextrin-iodine complex concentration (c_5) can be described empirically with a simple, single exponential decay, as $c_5 \div c_5\,(t = 0) = \exp(-\alpha t)$ (Fig. 2E), where α is the decay factor for the maltodextrin-iodine complex that depends on temperature. FEA investigations where we maintained diffusivity values at 30°C while permitting temperature shift alterations for reaction equilibrium constants demonstrated that both equilibrium constants and diffusivity values had major effects on the color decay rate with temperature variations (fig. S4, D and E).

Atomic mapping with EDS revealed the distribution of iodine in a cross section of a PDMS microchannel ($D = 0.68$ mm, $L = 40$ mm), through which iodine/iodide solution continuously flowed at 0.5 μl/min for 16 hours. The iodine concentration in PDMS exhibited a gradient from 0.4 wt % at the microchannel surface to 0 wt % at a radius of 1.6 mm (Fig. 2F). Visual inspection of the PDMS microfluidic device after the timer experiment showed yellow, trace iodine residues (fig. S5A). Ultraviolet-visible (UV-vis) spectroscopic measurements support this mechanism through decreasing characteristic absorbance of maltodextrin-iodine (fig. S5B) or iodine solution (fig. S5C) within microfluidic chambers with time and subsequent recovery upon the addition of iodine solution (fig. S5B).

Benchtop validation based on optical imaging (Fig. 2G) and reflectance UV-vis spectroscopy (fig. S5D) was conducted with a device that consisted of 11 sequential chambers designed for assessing accuracy and precision. The device was connected to a pumping system with an artificial sweat input of 0.5 μl/min, resulting in a time interval for filling neighboring reservoirs of 8 min. As expected, we saw a continuous gradation of color from the first to the last reservoirs over 120 min (Fig. 2G and fig. S5E). We evaluated the Commision Internationale de l'Eclairage L*a*b* (CIELAB) color space perceptual lightness (L*) of the colorimetric timer as a readout of the assay. A calibration curve of the in vitro assay was constructed to relate L* with collection time with a prediction accuracy of ±4.42 min (fig. S5F). The colorimetric timer supported testing scenarios where the participant stops the exercise and later resumes (fig. S5G). To test the performance of the colorimetric timer in vivo, we performed a 10-min iontophoresis, stimulation of sweat by delivering pilocarpine drug into the skin at 0.5 mA/cm^2, on a healthy human volunteer and then applied an 11-channel timer device to the stimulated area of skin. The device demonstrated a characteristic color gradient profile across the microfluidic reservoirs upon complete filling after 60 min (Fig. 2H). In this study, a liquid crystal thermochromic sensor inside the device calibrated for temperature variations (fig. S5, H and I). The device determined corresponding on-body sweat collection times with an accuracy of ±5 min (Fig. 2, I and J).

Sweat chemical composition can affect the behavior of the assay, so we tested for interaction between iodine and several common molecules found in sweat (fig. S6, A and B). In particular, uric acid in sweat can react with the iodine molecules of the timing assay, discoloring the assay by dissociating the maltodextrin-iodine complex (fig. S6C). The absorbance of maltodextrin-iodine (fig. S6D) and iodine (fig. S6E) decreased dose dependently with the addition of uric acid (fig. S6F). Accordingly, the addition of sacrificial contaminant-removing pads (CRPs) consisting of a shorter-chain maltodextrin and iodine complexes removed these interfering species, thereby decreasing these sources of variability (Fig. 2K and fig. S6, G and H). Shallow microfluidic chamber depth also reduces chemical interference by minimizing the amount of uric acid within the microfluidic chamber volume. As an additional control, sodium phosphate buffer at 0.1 M concentration stabilized the pH of the assay chamber (fig. S6I).

The plasmonic lactate sensor detects sweat lactate with multiwavelength changes

Quantitative determination of lactate concentrations in sweat relied on an enzymatic bioassay leveraging plasmonic AgNPLs as a colorimetric reporter, with immobilized lactate oxidase (LOX) as the biorecognition element (Fig. 3A and fig. S7A). The overall operating mechanism consisted of a molecular cascade wherein the oxidation of lactate from sweat by LOX produced H_2O_2, which reacted directly with uric acid under alkaline conditions. This reaction liberated free cyanuric acid that induced the etching of AgNPLs (Fig. 3, A and B) (*26*–*29*). H_2O_2 is largely inactive toward AgNPL etching in a highly alkaline environment with a redox potential of +0.867 V compared with +0.799 V for Ag^+ (*29*). Because the lactate sensor was constructed under high alkalinity within an agarose and polyethylene oxide (PEO) matrix to enhance AgNPL stability against salt, the cascade reaction was engineered to overcome this low activity by incorporating a high concentration of uric acid to enhance the responsiveness to H_2O_2 (Fig. 3B) (*29*). By adjusting the concentration of uric acid (fig. S7B), the wavelength (high aspect ratio; fig. S7C), and volume (fig. S7D), the response to H_2O_2 of the AgNPLs could be modulated to control the sensitivity. The reaction between AgNPLs and cyanuric acid preferentially etched the corners of the structures to yield truncated triangles (top right), then hexagons (bottom right), and eventually circular geometries (bottom left) (Fig. 3C). This morphological change led to a blue wavelength shift that depended on the concentration of H_2O_2 (Fig. 3D).

The sensor construction included a negatively charged polymeric LOX host layer to align the assay dynamic range with common lactate concentrations in human sweat by shielding the positively charged active site of LOX. This host layer consisted of PEO, bovine serum albumin (BSA), and chitosan (fig. S7A). An additional layer of cellulose acetate acted as a diffusion-limiting barrier to the sudden flux of lactate. The resulting sensor exhibited a standard calibration curve determined using artificial sweat with lactate concentrations between 0 and 20 mM (Fig. 3E). The linear range extended from 1 to 20 mM, with a limit of detection of 0.34 mM (Fig. 3E). The color change of the lactate sensor 30 min after the beginning of the reaction was 97.2 ± 1.6% with respect to the maximum color change (fig. S7E). This lactate sensor exhibited stability (Fig. 3F and fig. S7, F to H) and specificity (fig. S7, I to K) with minimal interference from other chemical species in sweat. A Coulombic steric barrier within the relevant stabilizing architecture (*30*–*33*) prevented etching and aggregation induced by NaCl, up to 100 mM.

The performance of the lactate assay depended on the pH of sweat, a parameter that can change during exercise. Three design features of the sensors minimized this effect. First, the cellulose acetate and PEO reduced proton diffusion in the vicinity of the enzyme (*11*, *34*). Second, the construction involved strong alkaline conditions, with a pH ≥ 10.5, thereby minimizing changes in pH

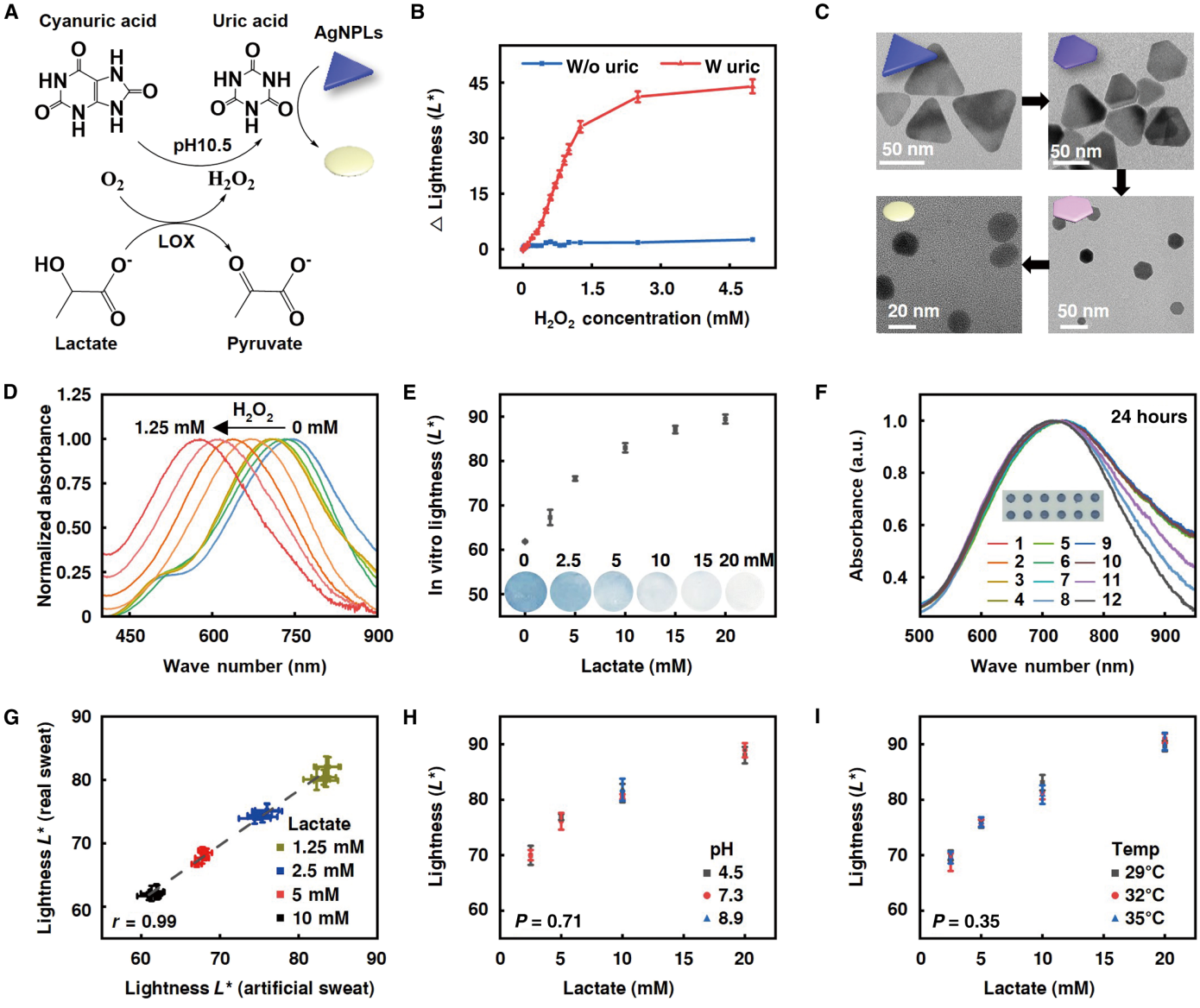

Fig. 3. Plasmonic colorimetric sensor detects lactate concentration. (**A**) Schematic illustration of the mechanism of the lactate sensor, highlighting the multilayer structure of lactate oxidase, AgNPLs hydrogel, and cellulose acetate. (**B**) Change in lightness (ΔL^*) from an initial value with and without uric acid as a function of H_2O_2. $n = 3$. (**C**) TEM image of AgNPLs, demonstrating the change in morphology from triangles into truncated nanotriangles, nanohexagons, and then to spheres because of etching by H_2O_2. Scale bars, 20 or 50 nm. (**D**) UV-vis spectra of AgNPL hydrogel after exposure to H_2O_2 from 0 to 1.25 mM. $n = 1$. (**E**) Standard calibration curve for the L^* of the sensor and corresponding optical images of the assay after exposure to lactate at concentrations between 0 and 20 mM. $n = 3$. (**F**) UV-vis spectral response for the effect of each of the major chemical components in sweat, after 24 hours of incubation. These major chemical components included 1, water; 2, 10 mM NaCl; 3, 25 mM NaCl; 4, 50 mM NaCl; 5, 75 mM NaCl; 6, 100 mM NaCl; 7, 100 mM glucose; 8, 100 mM lactate; 9, 10 mM uric; 10, 10 mM urea; 11, synthetic sweat; and 12, artificial sweat. $n = 1$. a.u., arbitrary units. (**G**) Comparison of sensor with artificial sweat and real sweat with different concentrations of added lactate. Pearson's correlation, $r = 0.99$, $n = 3$. (**H**) L^* as a function of lactate concentration in artificial sweat at physiologically relevant range of pH. $n = 3$. One-way ANOVA with Tukey's post hoc test. (**I**) L^* as a function of lactate concentration in artificial sweat at a physiologically relevant range of temperatures. $n = 3$. One-way ANOVA with Tukey's post hoc test. Data are presented as the mean ± SD. Schematics and illustrations created with Adobe Illustrator and Autodesk 3ds Max.

associated with incoming sweat (typically 4.5 to 8.9 in pH) (fig. S8A). Third, the use of cyanuric acid to etch AgNPLs, instead of H_2O_2, removed the pH-dependent effects inherent with H_2O_2 (*29*).

Evaluation of the sensor in practical applications used sweat from three adult participants spiked with additional lactate. Real human sweat produced similar colorimetric changes to artificial sweat in benchtop testing ($r = 0.99$) (Fig. 3G), and on-body colorimetric lactate sensor results correlated well with nuclear magnetic resonance (NMR)–based lactate measurements, with a Pearson's correlation factor of 0.82 (fig. S8B). We evaluated the lactate sensor under relevant ranges of pH and temperature. Measurements using artificial sweat with pH values of 4.5, 7.3, and 8.9 at 32°C exhibited

no significant pH dependence at 10 mM ($P = 0.71$) (Fig. 3H and fig. S8C). Similar studies also revealed no significant dependence on temperature across a range from 29° to 35°C at 10 mM lactate ($P = 0.35$) (Fig. 3I and fig. S8D).

Dye-conjugated SiO_2 nanoparticles in a hydrogel matrix produce a nonbleeding pH sensor

To evaluate sweat pH, we developed a reliable, nonbleeding colorimetric sensor of mesoporous SiO_2 particles loaded with BTB dye and embedded in an agarose hydrogel (Fig. 4A and fig. S9A). The porous particles had a uniform average size of approximately 376 ± 31.7 nm (Fig. 4B). The large surface area supported covalent bonding of BTB dye (Fig. 4C and fig. S9, B and C), as the basis for a nonbleeding pH assay, ensuring reliable performance by eliminating dye leakage to the surrounding fluid. The SiO_2 hydrogel sensor exhibited a response over a wide range of pH values, with a color shift from deep yellow at pH 4 to deep green at pH 8, with a coefficient of variation of 1.32% (Fig. 4D). The initial response reached 95% of the final color change within the first minute (fig. S9D). Spectral measurements revealed an increasing peak in absorbance at λ = 627 nm when exposed to standard buffers from pH 3 to pH 10 (Fig. 4E). The sensor displayed reversibility to alternating pH solutions between 5

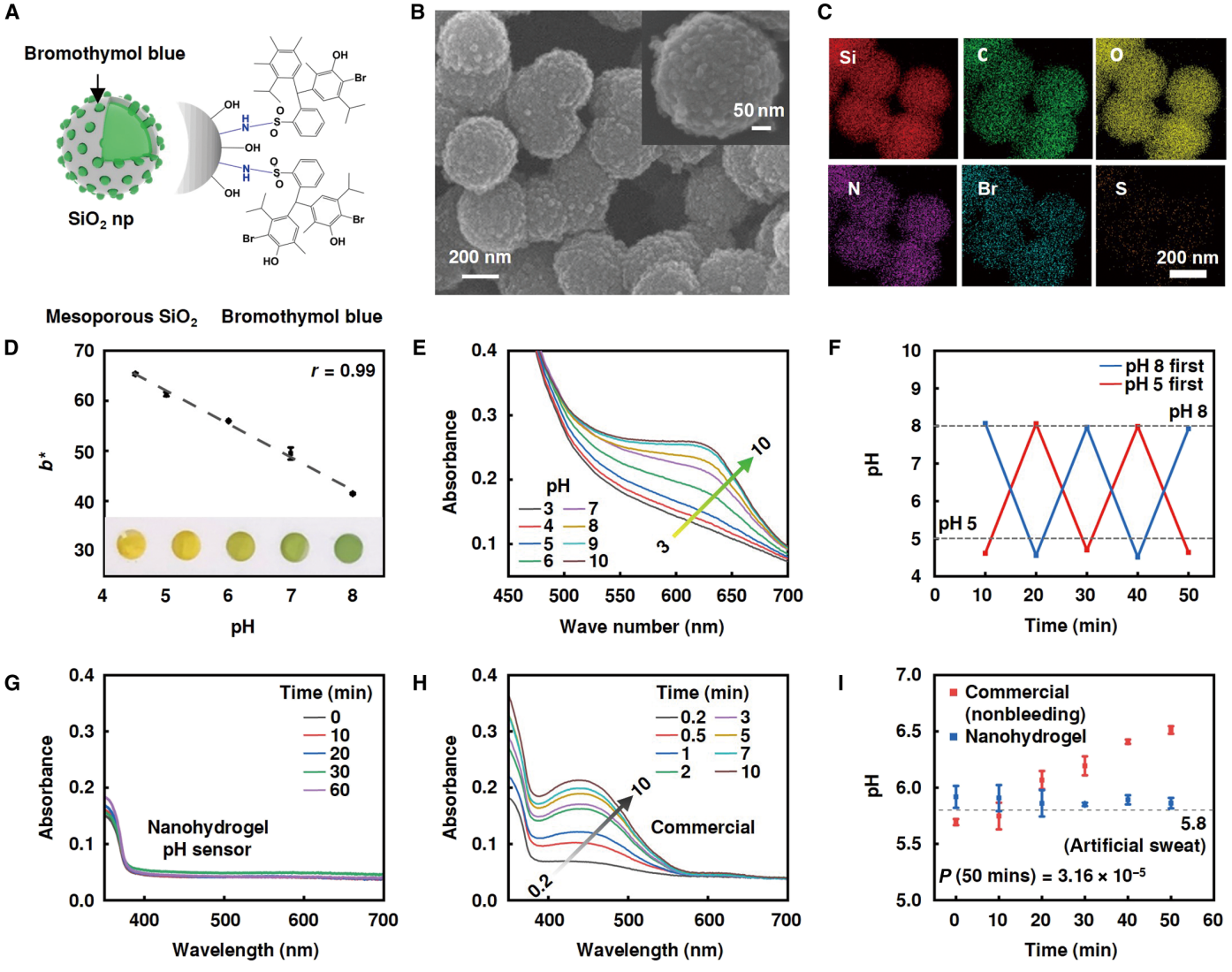

Fig. 4. Bromothymol blue–conjugated SiO_2 nanoparticles act as a reversible colorimetric pH sensor. (**A**) Schematic illustration of the sensor, highlighting mesoporous SiO_2 nanoparticles (np) chemically conjugated to bromothymol blue (BTB) dye. (**B**) SEM image of the mesoporous SiO_2 nanoparticles. Scale bars, 200 nm and 50 nm (inset). (**C**) SEM image with the elemental mapping profile of the BTB dye bonded with SiO_2. Si, silica; C, carbon; O, oxygen; N, nitrogen; Br, bromine; and S, sulfur. Scale bar, 200 nm. (**D**) Color (b^*) variation of the SiO_2 pH sensor in response to standard buffered solutions with pH values from 4 to 8 with optical images of the sensor. Pearson's correlation, $r = 0.99$, $n = 3$. (**E**) Absorbance of the sensor in response to different standard buffered solutions with pH values from 3 to 10. $n = 1$. (**F**) Performance of the sensor under cycling pH conditions between 5 and 8. $n = 3$. (**G** and **H**) UV-vis spectra of supernatant solution of (G) the SiO_2 pH sensor and (H) commercial pH paper as a function of incubation time with a standard buffer solution of pH 4. $n = 1$. (**I**) Comparison of pH as a function of time measured with the SiO_2 pH sensor and a nonbleeding commercial pH sensor within a microfluidic environment. $n = 3$. One-way ANOVA with Tukey's post hoc test. Schematic illustrations created with Autodesk 3ds Max and ChemDraw.

and 8 within a microfluidic well system (Fig. 4F), with the ability for reuse up to nine times (fig. S9E).

Further insight into the nonbleeding performance followed from measurements of the spectra of the pH 4 and 8 buffer solutions in contact with various types of pH sensors over 1 hour (Fig. 4, G and H, and fig. S9, F and G). The SiO_2 sensor, with covalently bonded BTB, showed no change after incubation with pH 4 (Fig. 4G) and pH 8 buffer (fig. S9H). When bulk BTB dye was simply mixed with agarose hydrogel without including SiO_2 nanoparticles, leakage occurred, as evidenced by an increase in absorbance (fig. S9I). The pH assay on a commercial bleeding pH paper exhibited an increase in absorbance because of dye leakage (Fig. 4H). In addition, the indicators can have a direct influence on the pH signal drift over time when the sweat volume to pH sensor surface area ratio is small. The SiO_2 sensor demonstrated significantly less drift in pH reading over 50 min compared with a commercially marketed nonbleeding pH paper ($P = 3.16 \times 10^{-5}$) (Fig. 4I).

Sweat pH provides information on exercise intensity, local muscle activation, and fitness

Next, a series of exercise studies using the skin-interfaced microfluidic band explored various sweat physiological parameters (Fig. 5A). Simultaneous measurements of blood lactate and the iontophoretically generated sweat pH provided insights into the interaction of sweat pH with surrounding blood and subsequently muscle tissues (fig. S10, A and B) (*35*, *36*). Ten-minute iontophoresis before each exercise session modulated sweat pH to be more neutral compared with exercise sweat, thereby enhancing changes related to exercise stimulus (Fig. 5B) (*37*) and allowed for the sampling of sweat at a consistent rate across different exercise intensities and at rest (fig. S10C) (*38*). The participants were asked to exercise by cycling at different targeted heart rates [90, 120, and 150 beats per minute (bpm)] for 20 min. Sweat was captured by the microfluidic band from locations where muscles were actively working (leg) or not working (arm). Collected data included heart rate, oxygen saturation (spO_2), and blood lactate, along with sweat rate, sweat pH, sweat lactate, and device temperature.

The pH of sweat collected from regions of working and nonworking muscles for six participants showed significantly different responses to exercise (120 bpm: $P = 0.001$, 150 bpm: $P = 0.013$) (Fig. 5, C to E). In nonworking muscles, sweat pH did not change with exercise intensity up to 120 bpm from sweat pH at rest (Fig. 5C), and the correlation between sweat pH and heart rate (fig. S10D) and blood lactate (Fig. 5D) was poor with Pearson's coefficients of 0.47 and 0.42, respectively. In contrast, iontophoretically derived sweat pH decreased gradually across different intensities of exercise from 7.3 (resting) to 5.5 (150 bpm) for working muscles, with a strong correlation to blood lactate concentration (Pearson's coefficient of −0.83, for 13 participants, 57 sessions) (Fig. 5E) and heart rate (Pearson's coefficient of −0.86, for 13 participants, 57 sessions) (fig. S10D). Sweat rate did not correlate with sweat pH for either working ($r = 0.15$) or nonworking muscles ($r = 0.20$) (fig. S10E). We next analyzed the interaction plots of variations in sweat pH for working and nonworking muscles correlated for different participants at four different heart rates (fig. S11). Before exercise and at a heart rate of 90 bpm, muscle activation did not have an effect on sweat pH ($P = 0.095$ and $P = 0.069$, respectively) (fig. S11, A and B). Muscle activation (nonworking versus working) significantly affected sweat pH when exercise was conducted at heart rates of 120 and 150 bpm ($P = 0.001$ and $P = 0.013$, respectively) (fig. S11, C and D). These results suggest that sweat pH relates to exercise intensity and to local muscle acidity.

Further studies associated with working muscles at varying cycling speeds indicated connections to personal fitness. These investigations involved 12 participants (eight males, four females) to test the effect of fitness on changes in sweat pH with exercise intensity (fig. S12A). We divided the participants into two fitness groups on the basis of their self-reported weekly exercise duration and blood lactate response to 14- to 19-mph cycling. Individuals were assigned to the "fit" group if they reported regular weekly exercise of >2 hours per week or the "unfit" group if they reported ≤2 hours per week. The male fit group had blood lactate concentrations less than 5 mM compared with the male unfit group with more than 7.5 mM when cycling at 19-mph speed (*39*). Likewise, the female fit group had blood lactate concentrations of less than 5 mM compared with the female unfit group with more than 6 mM when cycling at 14-mph speed (table S2). We evaluated the pH of sweat iontophoretically collected from working muscles during cycling at different speeds (9, 14, and 19 mph), along with heart rate, sweat rate, and blood lactate measurements (fig. S12, B and C). Two-way analysis of variance (ANOVA) of sweat pH for gender and fitness status showed that fitness status had significant effects on sweat pH for 9-, 14-, and 19-mph cycling speeds ($P = 1.1 \times 10^{-6}$, 2.0×10^{-9}, and 1.9×10^{-8}, respectively). There was no effect of gender on sweat pH at 0, 9, and 14 mph ($P = 0.79$, 0.39, and 0.15, respectively); however, at 19 mph, gender had a significant effect on sweat pH ($P = 1.6 \times 10^{-10}$) (Fig. 5F). Sweat pH remained unchanged for the fit male participants for speeds up to 19 mph. By contrast, the pH decreased for the unfit male and female participants (Fig. 5F). Fit female participants with a muscle mass of 24.9 ± 0.5 kg maintained steady sweat pH and blood lactate concentrations up to 14-mph cycling speed compared with unfit nonexercising male participants with a muscle mass of 31.4 ± 2.7 kg (Fig. 5, F and G).

Examination of the correlation between blood lactate and sweat pH followed different trends for fit and unfit participants (Fig. 5H). Sweat pH showed smaller changes with increasing blood lactate concentrations for fit participants than for unfit participants, consistent with previously reported findings for muscle pH (*40*) (fig. S12D). Examination of the correlation between heart rate and sweat pH also showed smaller changes in sweat pH with increasing heart rates for fit participants than for unfit participants (fig. S12E). Sweat pH did not correlate with the sweat rate for both fit ($r = 0.13$) and unfit participants ($r = 0.41$) (fig. S12F). Unlike sweat pH, there was no correlation between sweat lactate measured by NMR or the Ag-NPL sensor and blood lactate with Pearson's coefficients of −0.15 and −0.24, respectively (Fig. 5, I and J).

Investigation of sweat lactate responses for working and nonworking muscles showed no clear relationships before, during, or after cycling (fig. S13A). On the basis of NMR measurements (fig. S13B), sweat lactate did not change with exercise for either nonworking ($r = 0.11$) (fig. S13, C and D) and working muscles ($r = -0.15$) (Fig. 5I and fig. S13E) unlike blood lactate, which increased with cycling (fig. S13, C and E). Other biophysical parameters including heart rate (fig. S13F), sweat rate (fig. S13G), and sweat pH (fig. S13H) showed no clear relationship with sweat lactate. Time dynamic measurements showed decreasing sweat lactate concentrations after onset of sweating and no clear response to exercise or recovery (fig. S13, I to K).

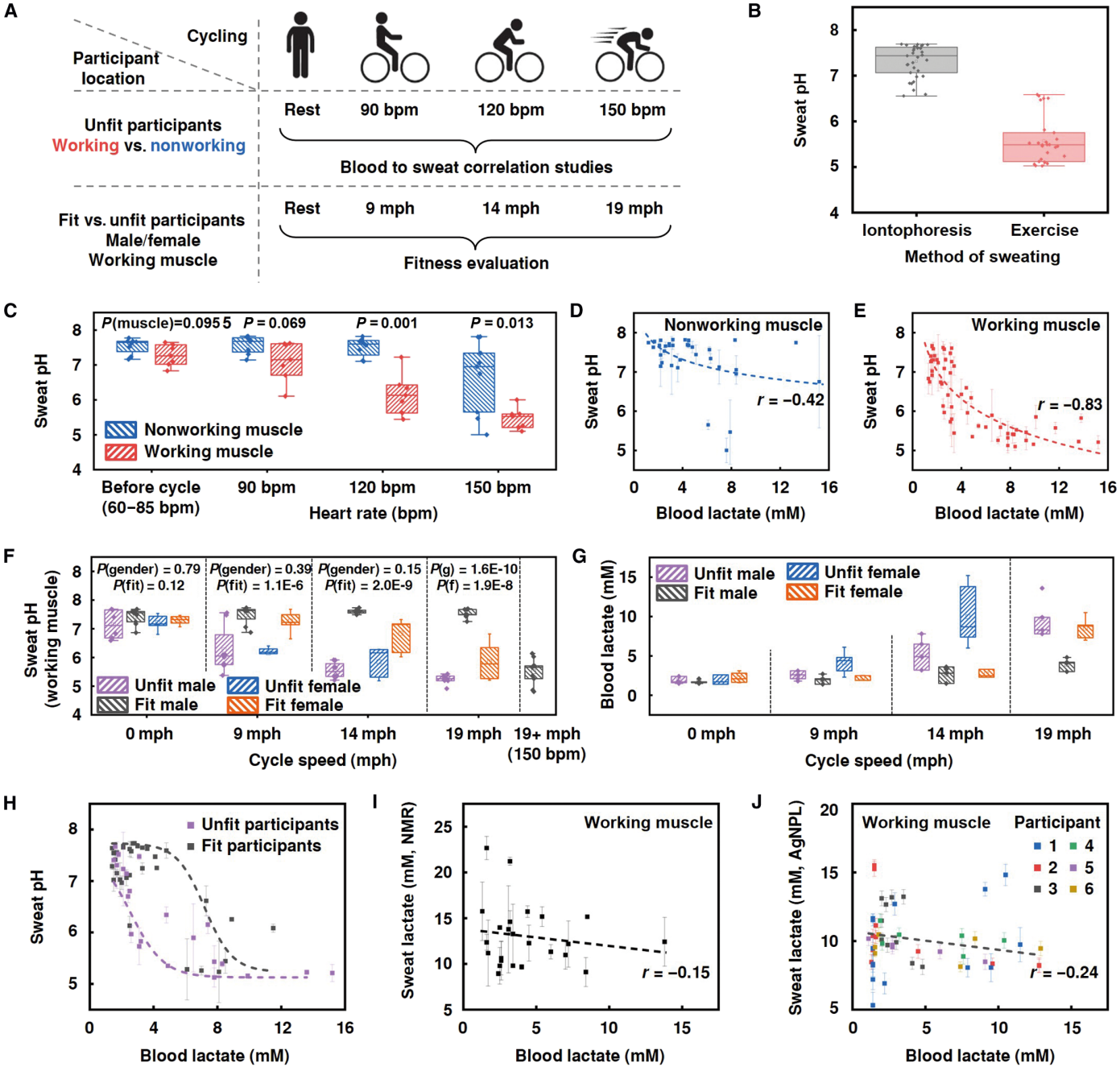

Fig. 5. Evaluation of sweat pH and sweat lactate for monitoring personal fitness on the basis of exercise intensity, sampling location, and fitness. (**A**) Experimental protocol with different cycle speeds for studies to correlate concentrations of lactate in blood, heart rate, and iontophoretically generated sweat pH and lactate in fitness evaluations. (**B**) Sweat pH analyzed by the sensor in samples collected by iontophoresis at rest ($n = 33$) or during exercise without iontophoresis ($n = 31$). (**C**) Sweat pH for various exercise intensities (no exercise, 90, 120, and 150 bpm) collected from regions of working (leg) and nonworking (arm) muscle. ($n = 12$, six participants and one device per condition, each box contains seven to nine data points.) Two-way ANOVA with Tukey's post hoc test. (**D** and **E**) Correlation between blood lactate and nonworking muscle (D) ($n = 6$, Pearson's correlation analysis, $r = -0.42$) and working muscle (E) sweat pH. ($n = 13$, exercise condition = 57 sessions, Pearson's correlation analysis, $r = -0.83$). (**F** and **G**) Sweat pH (leg) (F) and blood lactate (G) with cycle speeds (0, 9, 14, and 19 mph) for fit and unfit participants ($n = 12$, six fit, six unfit). Two-way ANOVA with Tukey's post hoc test. (**H**) Correlation of pH of sweat collected from regions of working muscle and blood lactate for the fit and unfit participants ($n = 12$, six fit, six unfit). (**I** and **J**) Correlation between blood lactate and sweat lactate measured by NMR (I) and a wearable nanoplasmonic sensor (J) for the working muscle ($n = 6$ participants). Data in (C), (F), and (G) are presented as box and whisker plots with the position of minimum, lower quartile, median, upper quartile, and maximum. Dots represent individual sweat pH and lactate measurements from each microfluidic chamber. Data were analyzed with Origin Pro. Data in (D), (H), (I), and (J) are presented as scatterplots and were analyzed with linear regression to produce Pearson's correlation. Error bars are defined as the SD of measurements per single-intensity exercise session.

Studies with fully integrated devices reveal time-dynamic exercise sweat physiology

Next, we leveraged the integrated microfluidic device with the colorimetric timer, lactate sensor, and pH sensor to collect and evaluate the chemical composition of sweat distributed across multiple different time points. Here, two male participants with self-reported exercise of less than 2 hours per week (unfit) (Fig. 6, A and B) and two male participants who routinely exercised greater than 2 hours per week (fit) (Fig. 6, C and D) were evaluated as they followed experimental protocols of a period of rest, cycling, and recovery while wearing the microfluidic band (Fig. 6, A to D). Cardiovascular fitness evaluations indicated that at 19-mph cycling speed, heart rate and blood lactate were 114 to 127 bpm and 3 to 4.2 mM or 143 to 162 bpm and 7.8 to 8.3 mM for the fit and unfit participants, respectively (table S2).

Sweat pH in the two unfit participants was 7.1 and 7.5 at rest. With exercise, sweat pH decreased to 5.5 and 6.25, respectively. After exercise, sweat pH recovered to between 6.9 and 7.5 (Fig. 6, A and B). Blood lactate concentration in unfit participants increased from 1.5 to 13 mM, and heart rate rose from 65 to 75 to 155 bpm and then returned to the baseline for both participants (Fig. 6, A and B). In contrast, the sweat pH of both fit participants remained between 7.3 and 7.6 before, during, and after exercise (Fig. 6, C and D). Blood lactate increased from 0.9 to 3 mM at rest to 2.9 to 4.8 mM during cycling as the heart rate increased from 85 to 88 bpm to 127 to 150 bpm (Fig. 6, C and D).

A final set of experiments that examine variations in sweat pH during squatting indicated that sweat pH can also change with anaerobic exercise. Tests involved analysis of iontophoresis-generated sweat from the working muscle of three participants after 100 squats over 10 min (Fig. 6E). Sweat lactate decreased slightly during this period (Fig. 6F). As with cycling, sweat pH was neutral at the resting state and decreased with exercise (Fig. 6F) as blood lactate (Fig. 6G) and heart rate (Fig. 6H) increased with squatting.

DISCUSSION

The contributions reported here are physiological insights related to correlations between sweat and blood chemistry for purposes of real-time monitoring of muscle activity and personal fitness. The elastic microfluidic band with colorimetric sensors and timers presents a noninvasive tool for monitoring the time dependence of sweat pH and its connection, through blood lactate, to personal fitness during various exercises. This band naturally interfaces with straps used with smartwatches in a reusable format and adds capabilities in simultaneous measurements of heart rate, spO_2, sweat collection times, lactate concentrations, and pH. These colorimetric assays offer distinct advantages over other existing wearable sweat analytical systems. The colorimetric timer enables time-dynamic measurements of sweat chemistry for colorimetric sensing systems through the analysis of a single digital image. The nanoplasmonic lactate sensor uses localized surface plasmon resonances to induce a shift in the extinction coefficient that produces multicolor changes with sweat lactate concentrations. The resistance of the sensor to interfering effects such as those associated with pH, light, salt, temperature, and sweat chemical species allows for an accurate readout of sweat chemistry under dynamically changing physical and chemical environments. This assay is also more cost-effective than previous designs because of its ability to operate at low concentrations of LOX (tables S3 and S4).

Physiological studies with this platform demonstrate the utility of sweat as a potential noninvasive alternative to blood lactate testing during exercise monitoring. Comprehensive multiparametric exercise trials revealed relationships between muscle activity and sweat chemistry. Correlation between blood lactate and sweat pH highlights the potential of sweat analytics for personal fitness monitoring ($r = -0.83$, $n = 13$, data points = 57). Gradual decreases in sweat pH with increasing exercise intensity suggested that sweat pH may serve as an indicator of muscle acidity, which is related to muscle fatigue.

Although blood lactate measurements are effective for monitoring overall muscle fatigue, they do not provide specific information on the local production of lactate at a given muscle region because blood circulates rapidly throughout the body and tends to eliminate local differences in concentration (*41*, *42*). On the other hand, sweat is sourced directly from the area of the muscle of interest and can thus offer relevant information on local muscle fatigue and acidity. Our investigation on working and nonworking muscles revealed that sweat dynamics can offer physiological insights into local muscle activity ($n = 12$, data points = 48). Sweat pH on working muscle correlated with blood lactate and changed with exercise. By contrast, sweat sourced from nonworking muscles did not correlate well with blood lactate and generally did not change with exercise. This ability to monitor local muscle activity may provide athletes with targeted training advice for a specific muscle of interest.

In our study, sweat pH was different between regularly exercising fit individuals and less active unfit individuals, supporting the potential of sweat pH as a proxy for blood lactate testing ($n = 12$, data points = 54). Fit individuals exhibited less variation in sweat pH with increasing cycling speed compared with unfit individuals. This observation agrees with conventional blood lactate testing where blood lactate exhibits less variation with exercise intensity for fit participants (*40, 43*). Further, different trends for the response of sweat pH with blood lactate for the fit and unfit participants suggest that fit participants may be better able to maintain pH homeostasis at elevated blood lactate concentrations. Previous work suggests that physical fitness influences the ability to maintain pH homeostasis during elevated blood lactate concentrations with enhanced mitochondrial respiratory capacity (*44*), skeletal muscle buffering capacity (*43*), and H^+/Na^+ cotransport (*45*). Therefore, changes in sweat pH during exercise may inform users of their physical fitness status.

Our study is not without limitations. Iontophoretically generated sweat has a different pH compared with sweat from natural exercise, which limits the usefulness of natural sweat for personal fitness evaluations. Future research on alternative sweat generation methods and the relationship between their sweat chemistry with exercise will improve the practicality of the device. The microfluidic design constrains the operation time to several hours, but design modifications may provide routes to bypass this limitation. The comparisons made here were limited by the number of participants, and further validation with larger and more diverse populations including athletes will establish the broader reliability and generalizability of the findings. Long-term studies are essential to understand how sweat pH correlates with fitness progression and whether it can reliably predict overtraining or injury risk. Investigating daily variations in sweat pH because of factors such as diet, hydration, and sleep may contribute to an understanding of its dynamic nature. Developing intervention strategies based on sweat pH monitoring to optimize

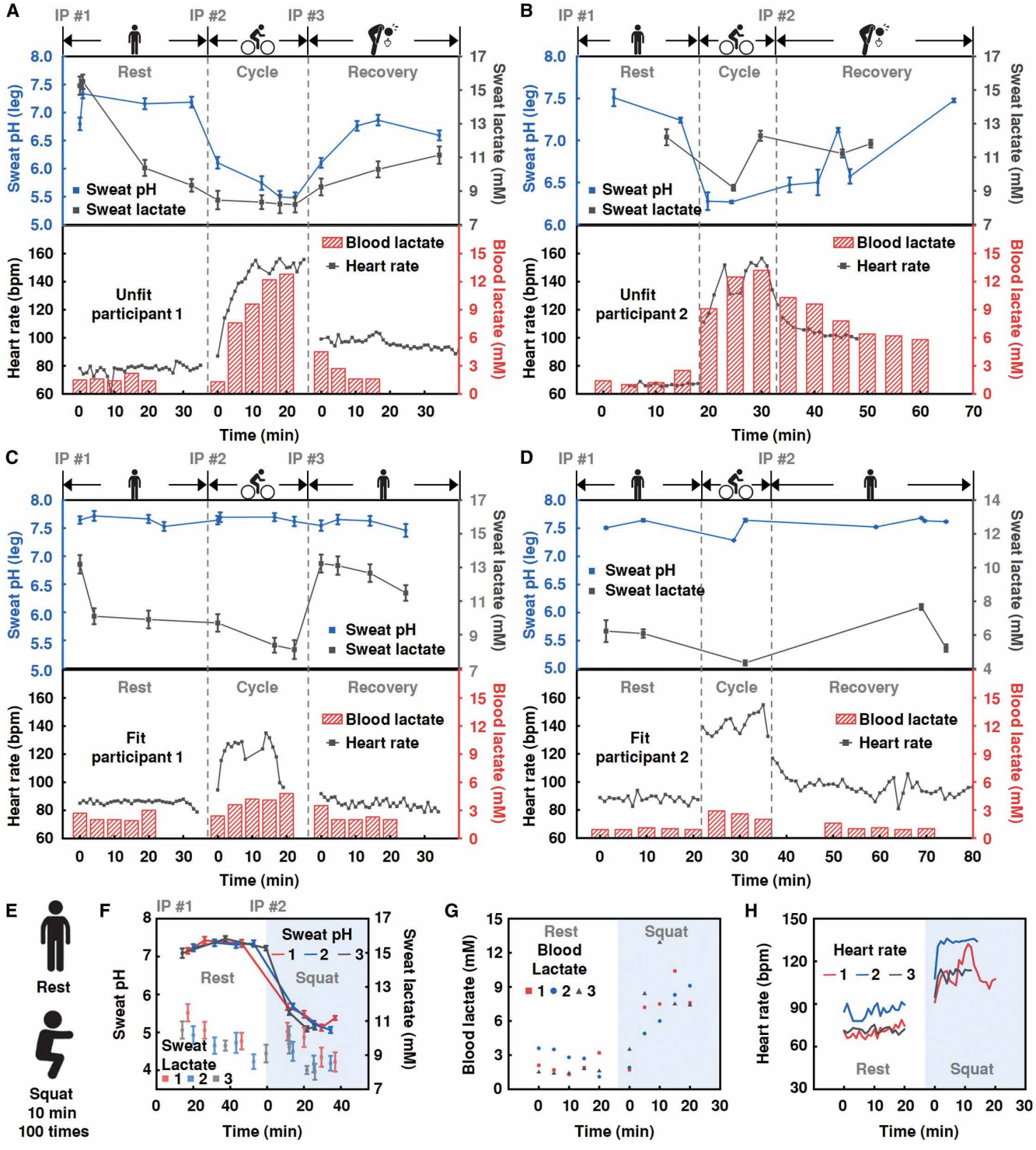

Fig. 6. Time-dynamic sweat exercise physiology using multifunctional sweat microfluidic devices with colorimetric timers. (**A** to **D**) Real-time monitoring of sweat pH (blue line) and sweat lactate (black line) collected from a region of working muscle and blood lactate (black line) and heart rate (red box) before, during, and after a session of cycling at 19 mph for the unfit participant 1 (A), the unfit participant 2 (B), and the fit participants 1 (C) and 2 (D). IP, 10-min iontophoresis session. (**E**) Exercise protocol for studying the effect of squatting on sweat pH. (**F** to **H**) Real-time monitoring of sweat pH and sweat lactate (F), blood lactate (G), and heart rate (H) before and during a squatting session. $n = 3$ participants.

fitness, training, and rehabilitation programs is also an important step for practical implementation.

The emergence of sweat acidity for muscle fatigue monitoring, using an adhesive-free wearable band, provides a new perspective for dynamic noninvasive sweat biochemical analysis during exercise. Other colorimetric assays or electrochemical sensors can be easily integrated into the platform reported here, to support expanded monitoring capabilities and enhanced tracking of exercise physiology. Engineering research and physiological studies in these directions offer great promise for continued work in this area.

MATERIALS AND METHODS

Study design

The objective of this study was to develop data to examine correlations of sweat pH and lactate concentration with blood lactate concentrations, muscle activity, and fitness using a sweat microfluidic band with a colorimetric timer, pH sensor, and lactate sensor for analyzing the physiological parameters related to the fitness of the participants. Testing was nonblinded and involved 14 healthy participants (aged 18 to 40) as volunteers. A priori power analysis for a two-tailed bivariate normal model correlation indicated that the minimum sample size to yield a statistical power of at least 0.8 with an alpha of 0.05 and a Pearson's correlation coefficient of 0.65 was 16. Human trials were approved by the Institutional Review Board (STU00214004-MOD0018) at Northwestern University, and all participants gave complete, informed, signed consent before participating in on-body experiments. No participants or outliers were excluded from the analysis. The exact participant numbers and data points used are indicated in the respective figure legends.

Fabrication of the microfluidic band

The band (157-mm by 16.5-mm rectangular strip) consisted of five layers: (i) a partially cured film of PDMS (thickness, 200 μm) to form the bottom part of the device, with a patterned area as a water-tight interface to the skin and a region through which sweat can enter the microfluidics (*46*); (ii) a PDMS microfluidic structure (thickness, 800 μm), formed by casting against molds formed by 3D printing, with a series of microfluidic channels, valves, and reservoirs in a linear array for sequential filling; (iii) colorimetric chemical reagents for assessing pH, lactate concentration, sweat temperature, and the colorimetric timer; (iv) a thin layer of PDMS to form a sealed top side; and (v) a film of PET with printed color reference markers selected to match the colorimetric reagents (Fig. 1A).

A 3D printer (Formlabs) was used to create clear resin-based molds (Resin Clear V4, Formlabs). Molds were cleaned by sonication in isopropyl alcohol twice for 2 min. A UV light cure for 15 min at room temperature completed the fabrication process. PDMS (Sylgard 184; mixing ratio of 20:1, Dow corning) was baked with white silicon dye (5 wt %, Reynolds Advanced Material) in the mold in a 75°C oven for 3 hours. Colorimetric assays were placed in the microfluidic reservoirs and capped with a thin PDMS. The 200-μm-thick capping layer was fabricated by spin-casting PDMS at 200 and 20 rpm on a poly(methyl methacrylate)–coated silicon wafer (silicon, 100-mm diameter, 500-μm thickness, UniversityWafer) and then baking at 95°C in an oven for 1 hour. Exposure to an oxygen plasma created hydrophilic surfaces that allowed for efficient bonding of the cap to the base. Blade coating of PDMS with a low cross-linking density (0.15 g, 30:1 ratio of base to curing agent, 30-mm length, 16.5-mm width) around the inlet of the band with PET tape masking at a predefined sweat collection area (8 mm by 12 mm) facilitated an adhesive-free, water-tight interface to the skin.

Preparation of the colorimetric timer

The colorimetric timer assay solution consisted of 2 wt % maltodextrin (dextrose equivalent 4.0 to 7.0, Sigma-Aldrich), 24 mM potassium iodide (KI), 3.1 mM I_2 (Sigma-Aldrich), and 0.1 M pH 5.5 sodium phosphate buffer. The substrate consisted of a cellulose paper (Whatman no. 602H, 125-mm diameter, 160-μm thickness, Cytiva) bonded to a double-sided diagnostic tape (9965, Acrylate, 86.4-μm thickness, 3MTM). A CO_2 laser [VersaLASER (VLS), Universal Laser Systems] cut the pressure sensitive adhesive (PSA)–cellulose paper into circular shapes (8-mm diameter) for loading 12 μl of the colorimetric assay solution and to engrave 2-mm by 2-mm cutting alignment marks. A razor blade (Personna Inc., 009RD razor blades) was used to cut the cellulose paper into a rectangular shape (2 mm by 2 mm). Nafion (0.75 μl, 1100 W, 5 wt %, Sigma-Aldrich) was added to the paper to form a perfluorinated coating around the cellulose fiber, followed by annealing at 75°C in an oven (Fisherbrand Isotemp, Thermo Fisher Scientific) for 30 min. A medical adhesive (9965 3MTM) bonded this assay to the PDMS at the locations of the reservoirs (2.5-mm square, 350-μm depth). The sacrificial CRP with a short-chain maltodextrin (dextrose equivalent 14.0 to 17.0, Sigma-Aldrich) and iodine was created by the same fabrication process. The decay factor was related to temperature (T) by $\alpha = 1.79 \times 10^{-4}\ T^2$ to $7.51 \times 10^{-3}\ T + 8.62 \times 10^{-2}$; α, 1/min; T, degrees Celsius; t, minutes; and $c_5(t)$, maltodextrin-iodine concentration at time t, millimolar.

Preparation of the lactate sensor

The AgNPLs were prepared as previously described (*47*), with slight modifications (Supplementary Materials). We prepared a stabilized solution of AgNPL by centrifugation of 10 ml of the AgNPL solution at 14,500 rpm for 40 min in a 15-ml tube and redispersion in 300 μl of 4% PEO (20 kDa, Sigma-Aldrich). The solid agarose AgNPL hydrogel was prepared by the addition of 75 μl of 0.3 M NaOH (Sigma-Aldrich) to 300 μl of agarose solution (320 mg/40 ml, Sigma-Aldrich) at 65°C in an Eppendorf tube. Subsequently, 300 μl of the AgNPL solution and 1000 μl of uric acid (10 mM dissolved in 75 mM NaOH, Sigma-Aldrich) were added to the agarose solution, completing the preparation of the AgNPL cocktail for molding. A total of 7.5 μl of this cocktail was poured into the PDMS mold (3-mm diameter, 1-mm depth) followed by drying at room temperature for 24 hours, which completed the solid agarose AgNPL hydrogel assay formation.

The microfluidic lactate sensor fabrication began with the preparation of a robust enzymatic solution by mixing 20 μl of a stock solution of 1000-U LOX (Toyobo Chemicals) with 980 μl of an enzymatic ink solution that consisted of 0.5% PEO, 0.05% BSA (Sigma-Aldrich), and 0.05% chitosan (Sigma-Aldrich). The LOX base layer was prepared by drop-casting of 5 μl of this mixture into each sensing reservoir (3-mm circle, 400-μm depth) and drying at 30°C for 1 hour. On top of the LOX base layer, we drop-casted 4 μl of 0.4% cellulose acetate (Sigma-Aldrich) in acetone followed by the AgNPL hydrogel (3-mm circular shape) placement in the chamber before the acetone dried out. After drying for 20 min, we completed the fabrication

process by drop-casting and drying another 4 μl of cellulose acetate (0.6% in acetone).

Preparation of the SiO_2 pH sensor

Mesoporous SiO_2 nanoparticles were synthesized by dissolving a solution containing 600 μl of tetraethyl orthosilicate and 1275 μl of 3-triethoxysilylpropylamine in 68.2 ml of a 1:1 ethanolic-to-water mixture and stirring at 600 rpm in a closed 100-ml vial. Subsequently, 6.75 ml of 0.2 M NaOH was added to the mixture and stirred for 1 hour at room temperature, and the SiO_2 nanostructures were collected by centrifugation at 10,000 rpm for 15 min and then redispersed in a 1:1 acetone-to-water mixture (63 ml). The sulfate group of BTB was converted to a sulfonyl chloride before attaching to the SiO_2. Initially, 4.16 g of BTB, 1.23 g of cyanuric chloride, and 0.67 g of triethylamine were dissolved in 90 ml of acetone, refluxed in a three-necked flask with stirring at 800 rpm for 3 hours at 65°C, and then cooled to ambient temperature to obtain activated BTB (a-BTB). Next, 5 ml of a-BTB was added to 31.5 ml of the SiO_2 suspension. The pH was adjusted to 9.5 using 2 M NaOH, and the reaction continued overnight at room temperature. The mixture was then centrifuged for 15 min at 10,000 rpm with two washes using an ethanolic solution to remove unbound BTB. Last, the SiO_2 loaded with BTB was dissolved in 7.4 ml of ethanol for further use. To create the SiO_2 pH sensor, 1 ml of the SiO_2 loaded with BTB suspension was centrifuged at 10,000 rpm for 15 min, redispersed in 1 ml of distilled water, and vigorously vortexed for 10 min. Subsequently, 300 μl of this suspension was mixed with 150 μl of a 4% PEO solution and 150 μl of an agarose solution (320 mg/ml) at 60°C. Next, 7.5 μl of the resulting mixture was drop-casted into a mold and allowed to dry overnight for pH sensing application.

Image processing and analysis

A Python-based analysis program (Epicore Biosystems) quantitatively analyzed images captured by a digital camera (EOS 6D, Canon) along with a color checker (24 color, Classic nano type, 24 mm by 40 mm, Calibrate). The calibration program extracted the CIELAB color coordinates from the red, green, blue (RGB) gray values of the digital images. Specifically, the user analyzed 24 different reference colors of known color coordinates and ran the transformation matrix to correct for the color differences induced by lighting conditions and the digital camera RGB sensor performances. Alternatively, a high-resolution color laser printer (Color ImageClass model, Canon) defined color reference markers at 1200–dots per inch (dpi) resolution on a 25-mm-thick PET film (FLX000464, FLEXcon), which can be compared against the microfluidic assays to semiquantitatively analyze the assays. An optical image of this device after exercise is shown in fig. S13L.

Iontophoresis

Ten milliliters deionized (DI) water and 400 mg of agarose [4% by weight fraction of the DI water added, type I, low electroendosmosis (EEO), Sigma-Aldrich] were mixed inside a 20-ml glass vial placed on a hot plate at 160°C with constant stirring (480 rpm). After cooling to 120°C, the addition of pilocarpine (Pilocarpine nitrate salt, Sigma-Aldrich) completed the preparation of the 0.5% weight fraction pilogel cocktail. Drop-casting the cocktail into cubic molds in PDMS (14 mm by 10 mm by 3 mm), followed by solidification at room temperature, completed the pilogel fabrication process. An in-house iontophoresis device, as previously described (*48*), was used to stimulate sweat for 10 min.

Studies of sweat pH on working muscle (thigh) versus nonworking muscle (forearm)

Six healthy volunteers participated in sweat pH testing for working and nonworking muscles. The on-body testing consisted of four separate exercise sessions with separate 10-min iontophoresis stimulation (0.5 mA, 0.5% pilogel) before each session: at rest, light exercise (90 bpm, 20 min), moderate exercise (120 bpm, 20 min), and intense exercise (150 bpm, 20 min). An alcohol swab was used to sanitize the skin before the devices were attached. Upon placement of the devices, participants were fitted with a commercial pulse oximeter (EMO-80, Emay) for continuous heart rate monitoring and started cycling (Gear 4, 250XL Upright Bike, XPLUS OUTDOOR). After 20 min, a commercial blood lactate reader (Lactate Pro 2 LT-1730, Akray) was used to measure blood lactate. After each session, operators captured images of the device on the skin with a digital camera. For sweat lactate correlation, microfluidic devices with a series of empty chambers sampled 3- to 4-μl volume of sweat for each time point. An NMR instrument (Bruker Neo 600 MHz system with a quadruple resonance cryoprobe (QCI-F cryoprobe) allowed highly sensitive temporal detection of sweat lactate concentrations.

Sweat physiology for fit and unfit participants

Six fit and six unfit volunteers participated in bicycle exercises, and information on the participant's exercise routines, body fat, weight, muscle mass, body mass index, and cardiovascular fitness was collected for each enrolled participant. Unfit participants were defined as individuals who exercised for 2 hours or less per week, whereas fit participants exercised more than 2 hours per week. The fit participants were able to maintain blood lactate concentrations of less than 5 mM while cycling at 19-mph speed (male participants) or 14-mph speed (female participants). Exercise protocols were the same as those for the working versus nonworking muscle tests, except that the cycle speed, instead of heart rate, modulated the exercise intensity; at rest, 9 to 10 mph, 14 to 15 mph, and 19 to 20 mph.

Integrated device for time-dynamic exercise physiology

For time-dynamic exercise physiology studies, the devices consisted of colorimetric timers, nanoplasmonic lactate sensors, colorimetric pH sensors, and colorimetric temperature sensors. Two fit and two unfit participants participated in each session and wore the sensor on the thigh. For two participants (one fit and one unfit), the protocol involved iontophoretically stimulating sweat (i) before cycling, (ii) during cycling at 19 mph for 20 min, and (iii) after recovery from cycling (Fig. 6, A and C). For the other two participants, the protocol involved iontophoresis sessions (i) before and during cycling at 19 mph for 20 min and (ii) after recovery from cycling (Fig. 6, B and D). For all participants, the operator captured images of the device using the digital camera 30 min after filling the required chambers (three to four sets of the timer, lactate sensor, and pH sensor). Three healthy participants participated in squat exercise tests to observe the effect of strength exercise on sweat pH. As with cycling, iontophoresis on the working muscle enabled sweat collection before and during squatting sessions (100 squats per person for 10 min). Blood lactate was sampled every 5 min, and heart rate was measured for the duration of the exercise sessions.

Statistical analysis

Statistical analyses used commercial software packages R (R Foundation for Statistical Computing) and Origin (Pro) (version 2022,

OriginLab Corporation). All measurements involved at least three repeats unless noted in the figure caption. Data are presented with mean values ± SD unless noted in the figure caption. Pearson correlation analyses were performed to evaluate relationships between the variables. A one-way ANOVA with Tukey's post hoc test was used to determine statistical significance. Two-way ANOVA with Tukey's post hoc test was used to determine the statistical significance for working and nonworking muscles. $P < 0.05$ was considered statistically significant. Data were not tested for normality. All tabular data are available in data file S1.

Supplementary Materials

The PDF file includes:
Materials and Methods
Figs. S1 to S13
Tables S1 to S4
References (*49*–*58*)

Other Supplementary Material for this manuscript includes the following:
Data file S1
MDAR Reproducibility Checklist

REFERENCES AND NOTES

1. R. A. Robergs, F. Ghiasvand, D. Parker, Biochemistry of exercise-induced metabolic acidosis. *Am. J. Physiol. Regul. Integr. Comp. Physiol.* **287**, R502–R516 (2004).
2. M. Hargreaves, L. L. Spriet, Skeletal muscle energy metabolism during exercise. *Nat. Metab.* **2**, 817–828 (2020).
3. G. A. Brooks, The science and translation of lactate shuttle theory. *Cell Metab.* **27**, 757–785 (2018).
4. P. J. Derbyshire, H. Barr, F. Davis, S. P. Higson, Lactate in human sweat: A critical review of research to the present day. *J. Physiol. Sci.* **62**, 429–440 (2012).
5. K. Van Hoovels, X. Xuan, M. Cuartero, M. Gijssel, M. Swaren, G. A. Crespo, Can wearable sweat lactate sensors contribute to sports physiology? *ACS Sens.* **6**, 3496–3508 (2021).
6. T. T. Luo, Z. H. Sun, C. X. Li, J. L. Feng, Z. X. Xiao, W. D. Li, Monitor for lactate in perspiration. *J. Physiol. Sci.* **71**, 26 (2021).
7. F. Tehrani, H. Teymourian, B. Wuerstle, J. Kavner, R. Patel, A. Furmidge, R. Aghavali, H. Hosseini-Toudeshki, C. Brown, F. Y. Zhang, K. Mahato, Z. X. Li, A. Barfidokht, L. Yin, P. Warren, N. Huang, Z. Patel, P. P. Mercier, J. Wang, An integrated wearable microneedle array for the continuous monitoring of multiple biomarkers in interstitial fluid. *Nat. Biomed. Eng.* **6**, 1214–1224 (2022).
8. P. Bollella, S. Sharma, A. E. G. Cass, R. Antiochia, Minimally-invasive microneedle-based biosensor array for simultaneous lactate and glucose monitoring in artificial interstitial fluid. *Electroanalysis* **31**, 374–382 (2019).
9. P. Bollella, S. Sharma, A. E. G. Cass, R. Antiochia, Microneedle-based biosensor for minimally-invasive lactate detection. *Biosens. Bioelectron.* **123**, 152–159 (2019).
10. J. R. Sempionatto, M. Lin, L. Yin, E. De la Paz, K. Pei, T. Sonsa-Ard, A. N. de Loyola Silva, A. A. Khorshed, F. Zhang, N. Tostado, S. Xu, J. Wang, An epidermal patch for the simultaneous monitoring of haemodynamic and metabolic biomarkers. *Nat. Biomed. Eng.* **5**, 737–748 (2021).
11. X. Xuan, C. Chen, A. Molinero-Fernandez, E. Ekelund, D. Cardinale, M. Swaren, L. Wedholm, M. Cuartero, G. A. Crespo, Fully integrated wearable device for continuous sweat lactate monitoring in sports. *ACS Sens.* **8**, 2401–2409 (2023).
12. K. H. Lee, Y. Z. Zhang, H. Kim, Y. Lei, S. Hong, S. Wustoni, A. Hama, S. Inal, H. N. Alshareef, Muscle fatigue sensor based on $Ti_3C_2T_x$ MXene hydrogel. *Small Methods* **5**, e2100819 (2021).
13. W. Gao, S. Emaminejad, H. Y. Y. Nyein, S. Challa, K. Chen, A. Peck, H. M. Fahad, H. Ota, H. Shiraki, D. Kiriya, D. H. Lien, G. A. Brooks, R. W. Davis, A. Javey, Fully integrated wearable sensor arrays for multiplexed in situ perspiration analysis. *Nature* **529**, 509–514 (2016).
14. J. Tu, J. Min, Y. Song, C. Xu, J. Li, J. Moore, J. Hanson, E. Hu, T. Parimon, T. Y. Wang, E. Davoodi, T. F. Chou, P. Chen, J. J. Hsu, H. B. Rossiter, W. Gao, A wireless patch for the monitoring of C-reactive protein in sweat. *Nat. Biomed. Eng.* **7**, 1293–1306 (2023).
15. L. Yin, M. Z. Cao, K. N. Kim, M. Y. Lin, J. M. Moon, J. R. Sempionatto, J. L. Yu, R. X. Liu, C. Wicker, A. Trifonov, F. Y. Zhang, H. J. Hu, J. R. Moreto, J. Go, S. Xu, J. S. Wang, A stretchable epidermal sweat sensing platform with an integrated printed battery and electrochromic display. *Nat. Electron.* **5**, 694–705 (2022).
16. A. Koh, D. Kang, Y. Xue, S. Lee, R. M. Pielak, J. Kim, T. Hwang, S. Min, A. Banks, P. Bastien, M. C. Manco, L. Wang, K. R. Ammann, K. I. Jang, P. Won, S. Han, R. Ghaffari, U. Paik, M. J. Slepian, G. Balooch, Y. Huang, J. A. Rogers, A soft, wearable microfluidic device for the capture, storage, and colorimetric sensing of sweat. *Sci. Transl. Med.* **8**, 366ra165 (2016).
17. J. Choi, A. J. Bandodkar, J. T. Reeder, T. R. Ray, A. Turnquist, S. B. Kim, N. Nyberg, A. Hourlier-Fargette, J. B. Model, A. J. Aranyosi, S. Xu, R. Ghaffari, J. A. Rogers, Soft, skin-integrated multifunctional microfluidic systems for accurate colorimetric analysis of sweat biomarkers and temperature. *ACS Sens.* **4**, 379–388 (2019).
18. L. B. Baker, J. B. Model, K. A. Barnes, M. L. Anderson, S. P. Lee, K. A. Lee, S. D. Brown, A. J. Reimel, T. J. Roberts, R. P. Nuccio, J. L. Bonsignore, C. T. Ungaro, J. M. Carter, W. Li, M. S. Seib, J. T. Reeder, A. J. Aranyosi, J. A. Rogers, R. Ghaffari, Skin-interfaced microfluidic system with personalized sweating rate and sweat chloride analytics for sports science applications. *Sci. Adv.* **6**, eabe3929 (2020).
19. S. Kim, B. Lee, J. T. Reeder, S. H. Seo, S. U. Lee, A. Hourlier-Fargette, J. Shin, Y. Sekine, H. Jeong, Y. S. Oh, A. J. Aranyosi, S. P. Lee, J. B. Model, G. Lee, M. H. Seo, S. S. Kwak, S. Jo, G. Park, S. Han, I. Park, H. I. Jung, R. Ghaffari, J. Koo, P. V. Braun, J. A. Rogers, Soft, skin-interfaced microfluidic systems with integrated immunoassays, fluorometric sensors, and impedance measurement capabilities. *Proc. Natl. Acad. Sci. U.S.A.* **117**, 27906–27915 (2020).
20. J. Choi, D. Kang, S. Han, S. B. Kim, J. A. Rogers, Thin, soft, skin-mounted microfluidic networks with capillary bursting valves for chrono-sampling of sweat. *Adv. Healthc. Mater.* **6**, 10.1002/adhm.201601355 (2017).
21. A. J. Bandodkar, J. Choi, S. P. Lee, W. J. Jeang, P. Agyare, P. Gutruf, S. Wang, R. A. Sponenburg, J. T. Reeder, S. Schon, T. R. Ray, S. Chen, S. Mehta, S. Ruiz, J. A. Rogers, Soft, skin-interfaced microfluidic systems with passive galvanic stopwatches for precise chronometric sampling of sweat. *Adv. Mater.* **31**, e1902109 (2019).
22. M. Dautta, L. F. Ayala-Cardona, N. Davis, A. Aggarwal, J. Park, S. Wang, L. Gillan, E. Jansson, M. Hietala, H. Ko, J. Hiltunen, A. Javey, Tape-free, digital wearable band for exercise sweat rate monitoring. *Adv. Mater. Technol.* **8**, 2201187 (2023).
23. R. Seghir, S. Arscott, Extended PDMS stiffness range for flexible systems. *Sens. Actuators A Phys.* **230**, 33–39 (2015).
24. S. Gupta, M. Dixit, K. Sharma, N. S. Saxena, Mechanical study of metallized polyethylene terephthalate (PET) films. *Surf. Coat. Technol.* **204**, 661–666 (2009).
25. S. Moulay, Molecular iodine/polymer complexes. *J. Polym. Eng.* **33**, 389–443 (2013).
26. Z. X. Cai, Z. L. Wang, Y. J. Xia, H. Lim, W. Zhou, A. Taniguchi, M. Ohtani, K. Kobiro, T. Fujita, Y. Yamauchi, Tailored catalytic nanoframes from metal-organic frameworks by anisotropic surface modification and etching for the hydrogen evolution reaction. *Angew. Chem. Int. Ed. Engl.* **60**, 4747–4755 (2021).
27. X. Li, S. W. Wang, B. K. Xu, X. Zhang, Y. H. Xu, P. Yu, Y. J. Sun, MOF etching-induced Co-doped hollow carbon nitride catalyst for efficient removal of antibiotic contaminants by enhanced perxymonosulfate activation. *Chem. Eng. J.* **441**, 136074 (2022).
28. C. S. Venable, The action of hydrogen peroxide upon uric acid. Second paper on hydrogen peroxide as a reagent in the purin group. *J. Am. Chem. Soc.* **40**, 1099–1120 (1918).
29. R. Rizo, J. M. Feliu, E. Herrero, New insights into the hydrogen peroxide reduction reaction and its comparison with the oxygen reduction reaction in alkaline media on well-defined platinum surfaces. *J. Catal.* **398**, 123–132 (2021).
30. L. Johnson, D. M. Gray, E. Niezabitowska, T. O. McDonald, Multi-stimuli-responsive aggregation of nanoparticles driven by the manipulation of colloidal stability. *Nanoscale* **13**, 7879–7896 (2021).
31. I. Fernando, Y. Zhou, Impact of pH on the stability, dissolution and aggregation kinetics of silver nanoparticles. *Chemosphere* **216**, 297–305 (2019).
32. K. I. Peterson, M. E. Lipnick, L. A. Mejia, D. P. Pullman, Temperature dependence and mechanism of chloride-induced aggregation of silver nanoparticles. *J. Phys. Chem. C* **120**, 23268–23275 (2016).
33. J. P. Vivek, I. J. Burgess, Insight into chloride induced aggregation of DMAP-monolayer protected gold nanoparticles using the thermodynamics of ideally polarized electrodes. *J. Phys. Chem. C* **112**, 2872–2880 (2008).
34. X. Xuan, C. Pérez-Ràfols, C. Chen, M. Cuartero, G. A. Crespo, Lactate biosensing for reliable on-body sweat analysis. *ACS Sens.* **6**, 2763–2771 (2021).
35. P. A. Tesch, W. L. Daniels, D. S. Sharp, Lactate accumulation in muscle and blood during submaximal exercise. *Acta Physiol. Scand.* **114**, 441–446 (1982).
36. M. A. Komkova, A. A. Eliseev, A. A. Poyarkov, E. V. Daboss, P. V. Evdokimov, A. A. Eliseev, A. A. Karyakin, Simultaneous monitoring of sweat lactate content and sweat secretion rate by wearable remote biosensors. *Biosens. Bioelectron.* **202**, 113970 (2022).
37. F. Herrmann, L. Mandol, Studies of Ph of sweat produced by different forms of stimulation. *J. Invest. Dermatol.* **24**, 225–246 (1955).
38. K. Sahlin, R. C. Harris, B. Nylind, E. Hultman, Lactate content and pH in muscle obtained after dynamic exercise. *Pflugers Arch.* **367**, 143–149 (1976).
39. L. Vanhees, J. Lefevre, R. Philippaerts, M. Martens, W. Huygens, T. Troosters, G. Beunen, How to assess physical activity? How to assess physical fitness? *Eur. J. Cardiovasc. Prev. Rehabil.* **12**, 102–114 (2005).

40. J. H. Park, R. L. Brown, C. R. Park, M. Cohn, B. Chance, Energy metabolism of the untrained muscle of elite runners as observed by 31P magnetic resonance spectroscopy: Evidence suggesting a genetic endowment for endurance exercise. *Proc. Natl. Acad. Sci. U.S.A.* **85**, 8780–8784 (1988).
41. M. J. Comeau, T. M. Adams, J. B. Church, M. M. Graves, P. M. Lawson, Prediction of lower extremity lactate levels in exercising muscle utilizing upper extremity sampling sites. *J. Exerc. Physiol.* **14**, 20–27 (2011).
42. P. Foxdal, A. Sjodin, B. Ostman, B. Sjodin, The effect of different blood sampling sites and analyses on the relationship between exercise intensity and 4.0 mmol.l-1 blood lactate concentration. *Eur. J. Appl. Physiol. Occup. Physiol.* **63**, 52–54 (1991).
43. C. Juel, Muscle pH regulation: Role of training. *Acta Physiol. Scand.* **162**, 359–366 (1998).
44. C. Porter, P. T. Reidy, N. Bhattarai, L. S. Sidossis, B. B. Rasmussen, Resistance exercise training alters mitochondrial function in human skeletal muscle. *Med. Sci. Sports Exerc.* **47**, 1922–1931 (2015).
45. C. Juel, Lactate/proton co-transport in skeletal muscle: Regulation and importance for pH homeostasis. *Acta Physiol. Scand.* **156**, 369–374 (1996).
46. Z. Gu, X. Z. Wan, Z. Lou, F. L. Zhang, L. X. Shi, S. H. Li, B. Dai, G. Z. Shen, S. T. Wang, Skin adhesives with controlled adhesion by polymer chain mobility. *ACS Appl. Mater. Inter.* **11**, 1496–1502 (2019).
47. C.-Y. Kim, S. M. Shaban, S.-Y. Cho, D.-H. Kim, Detection of periodontal disease marker with geometrical transformation of Ag nanoplates. *Anal. Chem.* **95**, 2356–2365 (2023).
48. J. Kim, S. Oh, D. S. Yang, L. Rugg, R. Mathur, S. S. Kwak, S. Yoo, S. Li, E. E. Kanatzidis, G. Lee, H. J. Yoon, Y. Huang, R. Ghaffari, S. A. McColley, J. A. Rogers, A skin-interfaced, miniaturized platform for triggered induction, capture and colorimetric multicomponent analysis of microliter volumes of sweat. *Biosens. Bioelectron.* **253**, 116166 (2024).
49. J. C. Thompson, E. Hamori, Kinetic investigation of the amylose-iodine reaction. *J. Phys. Chem.* **75**, 272–280 (1971).
50. R. W. Ramette, R. W. Sandford, Thermodynamics of iodine solubility and triiodide ion formation in water and in deuterium oxide. *J. Am. Chem. Soc.* **87**, 5001–5005 (1965).
51. M. Yamamoto, T. Sano, T. Yasunaga, Interaction of amylose with iodine .I. Characterization of cooperative binding isotherms for amyloses. *Bull. Chem. Soc. Jpn.* **55**, 1886–1889 (1982).
52. G. Schwarz, On the analysis of linear binding effects associated with curved scatchard plots. *Biophys. Chem.* **6**, 65–76 (1976).
53. L. Cantrel, R. Chaouche, J. ChopinDumas, Diffusion coefficients of molecular iodine in aqueous solutions. *J. Chem. Eng. Data* **42**, 216–220 (1997).
54. A. W. Martinez, S. T. Phillips, E. Carrilho, S. W. Thomas, H. Sindi, G. M. Whitesides, Simple telemedicine for developing regions: Camera phones and paper-based microfluidic devices for real-time, off-site diagnosis. *Anal. Chem.* **80**, 3699–3707 (2008).
55. C. A. Chaplan, H. T. Mitchell, A. W. Martinez, Paper-based standard addition assays. *Anal. Methods* **6**, 1296–1300 (2014).
56. O. Faude, W. Kindermann, T. Meyer, Lactate threshold concepts. *Sports Med.* **39**, 469–490 (2009).
57. N. Promphet, P. Rattanawaleedirojn, K. Siralertmukul, N. Soatthiyanon, P. Potiyaraj, C. Thanawattano, J. P. Hinestroza, N. Rodthongkum, Non-invasive textile based colorimetric sensor for the simultaneous detection of sweat pH and lactate. *Talanta* **192**, 424–430 (2019).
58. W. He, C. Wang, H. Wang, M. Jian, W. Lu, X. Liang, X. Zhang, F. Yang, Y. Zhang, Integrated textile sensor patch for real-time and multiplex sweat analysis. *Sci. Adv.* **5**, eaax0649 (2019).

Acknowledgments: This work was supported by the Querrey-Simpson Institute for Bioelectronics at Northwestern University. This work made use of the EPIC facility of Northwestern University's NUANCE Center, which has received support from the SHyNE Resource (NSF ECCS-2025633), the IIN, and Northwestern's MRSEC program (NSF DMR-2308691). This work was supported by the Northwestern University High Throughput Analysis Laboratory and Keck Biophysics facility, the shared resource of the Robert H. Lurie Comprehensive Cancer Center of Northwestern University, supported partly by the NCI Cancer Center (support grant #P30 CA060553). We acknowledge the use of the facility at IMSERC at Northwestern University, which has received support from SHyNE Resource NSF ECCS-2025633 and NIH 1S10OD012016-01/1S10RR019071-01A1. **Funding:** We acknowledge support from the National Research Foundation of Korea (NRF) (2020R1A5A1018052 to D.-H.K., RS-2024-00346003 to D.-H.K., and RS-2024-00410209 to S.M.S.) and the Ministry of Trade, Industry, and Energy in Korea (P0017305 to D.Y. and D.-H.K. and RS-2024-00435693 to D.-H.K.). **Author contributions:** S.C., S.M.S., D.-H.K., and J.A.R. conceived the project, and Y.H., D.-H.K., and J.A.R. supervised the research. S.C., R.S., S.M.S., D.-H.K., and J.A.R. designed the research. J.A.R. conceptualized the wearable sweat band, and S.C. and R.S. developed and characterized the wearable sweat band. H.Z., X.L., and Y.H. performed FEA simulations for the mechanical deformation of the wearable sweat band. S.C. and R.S. developed and characterized the colorimetric timer, and H.Z., and Y.H. performed FEA simulations for the timer. S.M.S., S.C., S. Shajari, and R.S. developed and characterized the plasmonic lactate sensor. M.-J.K., S.M.S., S.C., and R.S. developed the SiO_2 pH sensor. D.Y. implemented the colorimetric temperature sensor. S.C., S.M.S., R.S., M.-J.K., D.Y., S.W., G.G., Y.X., S.Z., J.K., J.S., K.M., Z.C., M. Li, M. Lee, R.F.N., T.K., J.W., S. Shajari, and S. Son assisted in the exercise testing. S.C. and S.Z. performed statistical analysis. A.J.A. developed codes for colorimetric analysis. D.E.W. and R.G. provided sweat collection equipment and devices. S.C., S.M.S., R.S., H.Z., Y.H., D.-H.K., and J.A.R. wrote the original draft and edited the manuscript for review. **Competing interests:** A.J.A., D.E.W., and R.G. are employed by Epicore Biosystems. A.J.A., R.G., and J.A.R. are cofounders of a company, Epicore Biosystems, which develops and commercializes microfluidic devices for sweat analysis. All other authors declare that they have no competing interests. **Data and materials availability:** All data associated with this study are present in the paper or the Supplementary Materials. Device design for the wearable band is available at https://doi.org/10.5281/zenodo.13294830. All code related to the analysis presented is available at https://doi.org/10.5281/zenodo.13294802.

Submitted 7 February 2024
Resubmitted 14 June 2024
Accepted 15 August 2024
Published 4 September 2024
10.1126/scitranslmed.ado5366